Title	**Three-dimensional printing-based electro-millifluidic devices for fabricating multi-compartment particles**
Author(s)	**Chen, QL; Liu, Z; Shum, HC**
Citation	**Biomicrofluidics, 2014, v. 8 n. 6, article no. 064112**
Issued Date	**2014**
URL	**http://hdl.handle.net/10722/219123**
Rights	**Biomicrofluidics. Copyright © American Institute of Physics.**

Three-dimensional printing-based electro-millifluidic devices for fabricating multi-compartment particles

Qiu Lan Chen, Zhou Liu, and Ho Cheung Shum

Three-dimensional printing-based electro-millifluidic devices for fabricating multi-compartment particles

Qiu Lan Chen (陈秋兰),[a] Zhou Liu (刘洲), and Ho Cheung Shum (岑浩璋)[b]
HKU-Shenzhen Institute of Research and Innovation (HKU-SIRI), Shenzhen, Guangdong 51800, China and Department of Mechanical Engineering, The University of Hong Kong, Haking Wong Building, Pokfulam, Hong Kong

In this work, we demonstrate the use of stereolithographic 3D printing to fabricate millifluidic devices, which are used to engineer particles with multiple compartments. As the 3D design is directly transferred to the actual prototype, this method accommodates 3D millimeter-scaled features that are difficult to achieve by either lithographic-based microfabrication or traditional macrofabrication techniques. We exploit this approach to produce millifluidic networks to deliver multiple fluidic components. By taking advantage of the laminar flow, the fluidic components can form liquid jets with distinct patterns, and each pattern has clear boundaries between the liquid phases. Afterwards, droplets with controlled size are fabricated by spraying the liquid jet in an electric field, and subsequently converted to particles after a solidification step. As a demonstration, we fabricate calcium alginate particles with structures of (1) slice-by-slice multiple lamellae, (2) concentric core-shells, and (3) petals surrounding the particle centers. Furthermore, distinct hybrid particles combining two or more of the above structures are also obtained. These compartmentalized particles impart spatially dependent functionalities and properties. To show their applicability, various ingredients, including fruit juices, drugs, and magnetic nanoparticles are encapsulated in the different compartments as proof-of-concepts for applications, including food, drug delivery, and bioassays. Our 3D printed electro-millifluidic approach represents a convenient and robust method to extend the range of structures of functional particles. © 2014 AIP Publishing LLC. [http://dx.doi.org/10.1063/1.4902929]

I. INTRODUCTION

Compartmentalized particles consist of multiple compartments arranged into different configurations; each compartment may have dissimilar ingredients and unique properties, such as porosity or surface chemistry.[1,2] Multi-compartment particles are of interest for transporting several compounds for a wide range of applications, such as drug delivery, protein identification, cosmetics, food industry, and imaging.[3–9] Ingredients, including dyes, drugs, flavors, perfume, and peptides can be selectively encapsulated in pre-determined compartments. Spatially structuring the functional units within a particle potentially enables novel application of the resultant particles. For example, compartments can be designed to respond to different stimuli, such as magnetic fields, enabling on-demand sequential release.[1–3] Thus, the ability to engineer complex particles with multiple functionalities to meet the needs for novel applications is of key importance. Millimeter-sized compartmentalized particles enjoy reduced reagent consumption when compared with macroscopic particles, and yet contain a larger quantity of the encapsulated actives than microparticles. Therefore, their promise for use in applications in droplet-based sensing, encapsulation, and release is increasingly recognized.[10,11]

---

[a]Present address: Guangzhou Institute of Advanced Technology, Chinese Academy of Sciences, Guangzhou, China.
[b]Electronic mail: ashum@hku.hk

8, 064112-1

To make these multi-compartment particles with a complex architecture, devices with a complex structure are needed. Conventional capillary droplet microfluidics,[12–19] lithographic microfluidics,[20–24] and electrospray[25–30] show the capability in making compartmentalized particles with tunable size. For instance, core-shell, Janus, and even triphasic particles have been successfully fabricated and used in applications, such as preparation of polymer vesicles,[18] controlled drug release,[19,20] and encapsulation of fluorescent dyes.[31,32] However, particles with even more complex structures, such as core-shell particles with compartmentalized shells, demand devices with structures too sophisticated to fabricate and operate with conventional approaches. For instance, in capillary microfluidics and electrospray, the manual nature of the fabrication method and tedious assembly procedures often challenge the reproducibility in assembling devices with complicated geometries, which are typically needed for fabricating particles with more than two compartments. These devices can be more precisely fabricated using lithographic fabrication, where multiple device layers are fabricated and treated through a series of steps, including photolithography, replica molding, plasma treatments, and bonding.[22–24] To generate multi-compartment particles with sophisticated 3D structures, the multiple monolithic layers need to be accurately aligned and bonded to form interconnected channels across the different layers. The precision required in these steps demands tedious operating procedures, hampering the use of the technique for preparing truly three-dimensional particles with a complex architecture. Therefore, these conventional techniques have not been widely adopted for generating complicated particles, limiting their wider use in applications.

Recently, stereolithographic 3D printing has shown excellent potential for rapid prototyping of 3D structures, suggesting a new way to fabricate sophisticated devices with complex structures.[33–39] Liquid photopolymer is selectively polymerized according to the 3D design and the supporting material is removed to define the structures of the printed objects. With this approach, 3D devices can be directly realized without the need for lithographic masks, and steps, such as alignment and bonding of the individual components. Thus, it represents a convenient method to make millifluidic devices with channels in the millimeter size scale, which are difficult to achieve by either microfabrication or macrofabrication technologies. 3D printing has been used to fabricate molds for PDMS-based microfluidic devices,[33] reaction chambers for chemical synthesis,[34] and to achieve micromixing, isotachophoresis, and electrochemical detection.[35,36] However, the use of 3D printing to fabricate millifluidic devices for engineering particles with sophisticated structures remains unexplored.

In this paper, we introduce a 3D printing-based electro-millifluidic approach for synthesizing multi-compartment particles with designer 3D morphologies. By taking advantage of the ability of 3D printing to directly convert conceptual designs to prototypes, millimeter-sized channel networks with tunable size and customizable structures can be easily fabricated. Due to the laminar nature of the flow, tailored patterns formed by coflowing multiple fluid phases with different compositions can be easily realized. To enhance the size control using this approach, we incorporate electric field in the droplet generation. As a demonstration, we fabricate alginate hydrogel particles with multiple inner and phasic compartments arranged in sandwich-like, concentric, petal, and hybrid structures. A variety of ingredients, including fruit juices, drugs and magnetic nanoparticles, are encapsulated in the different compartments, to achieve co-encapsulation and release as well as spatially dependent actuation. By suggesting a new way to fabricate complicated particles, our work inspires novel applications of these particles in areas ranging from food to drug delivery and bioassays.

II. EXPERIMENTAL DETAILS

A. Material preparation

1.0% (w/w) sodium alginate (Aladdin Chemistry Co., Ltd, China) dissolved in DI water or fruit juice is prepared as the precursor solution by magnetic stirring for about 1 h. It has a viscosity of 111.1 mPa S at room temperature (μVISC^{TM}, RheoSense, Inc.). Afterwards, aqueous color dyes (Spotliter, Pilot, Japan) with different emission wavelengths are added to the precursor solution for visualization of the compartmental structures of the generated particles. The

green and red dye has a maximum excitation at wavelengths of 365 nm and 546 nm, respectively. The generated alginate droplets are cross-linked by divalent cations to form hydrogels in a water bath containing 3.0 wt. % calcium chloride (Sigma Aldrich, USA) solution. To form magnetized particles, the iron (III) oxide nanoparticles (Stock #: US3210, US Research Nanomaterials, Inc., USA) with sizes of 20–40 nm are encapsulated in the multi-compartment particles. To demonstrate the release of multiple drugs, we encapsulate vitamin C (Guangdong Nanguo Pharmaclline Co. Ltd., China, Approval No.: H44022547) and aminophylline (APL) (Shantou Jinshi General Pharmaceutical Factory, China, Approval No.: H44021063) in multi-compartment particles. The absorbance of the drugs released from the particles is measured using a UV-Vis spectrometer (NanoDrop 2000c, Thermo Scientific). The concentrations of aminophylline and vitamin C in their mixture change linearly with the absorbance at their corresponding wavelengths of 205 nm and 247 nm (Figs. S1 and S2 in the supplementary material).[40] The absorption signals of the two drugs do not interfere with each other, ensuring the validity of the release profiles from particles co-encapsulating both drugs (Fig. S2 in the supplementary material).[40] The surface properties of the millifluidic devices are characterized using a surface profiler (DektakXT, Bruker, Germany).

B. 3D printed device fabrication

Devices were designed in Pro/Engineer Wildfire 5.0 (Parametric Technology Corporation, MA, USA). The files containing the drawings of the parts were converted to .STL file for subsequent printing using an Objet Eden 350 V 3D printer. The liquid photopolymer is selectively polymerized according to the 3D design and the supporting material is drained to form the structures of the millifluidic devices. The transparent material, VeroClear, which is a proprietary acrylate-based photopolymer, acts as a base material to build the device. The white FullCure 705 is a non-toxic gel-like material, and acts as a supporting material to fill the hollow features during the preparation; it can be removed by repeated sonication and magnetic stirring in a sodium hydroxide solution. After the supporting material is thoroughly removed, syringe needles are glued to the inlets using 5 Minute® Clear Epoxy (VersaChem, Inc., USA) for injection of solutions through a plastic tubing (#BB31695-PE/5, Scientific Commodities, Inc., AZ). The device can also be covalently bonded with the commonly used optical adhesive film (MicroAmp, Catalog No.: 4311971, Applied Biosystems, CA), which is optically transparent and biocompatible. The fluidic samples are driven through the inlets into the devices using syringe pumps (Model Lsp01-2A, Baoding Longer Precision Pump Co., Ltd.).

C. Electrospray droplet generation

To achieve multi-compartment particles with controlled sizes, we spray the liquid jet formed by 3D printed device under an electric field (Fig. 1). When a high voltage is applied, the liquid jet will be stretched by the electric stress and adopt a tapered jet. Afterwards, the tapered jet will break up into uniform alginate droplets, which are collected in a bath of calcium chloride solution. The alginate droplets are subsequently cross-linked by calcium ions and form calcium alginate hydrogel particles.

III. RESULTS AND DISCUSSIONS

A. Characterization of 3D printed device

To make devices with millimeter-sized structures using conventional lithographic microfabrication technologies, multiple individual pieces with 2D features or layer-by-layer 2D features are typically first fabricated, followed by stacking, alignment, and assembly. With these conventional approaches, complex structures with non-contact overhanging parts or embedded inner features are difficult to achieve. This can be solved by adopting stereolithographic 3D printing into the fabrication process. The stereolithographic 3D printing used in this work is a bottom-up method based on the PolyJet technology.[41] The base and supporting materials are sequentially deposited onto a printer tray layer-by-layer with a thickness defined by the design. The
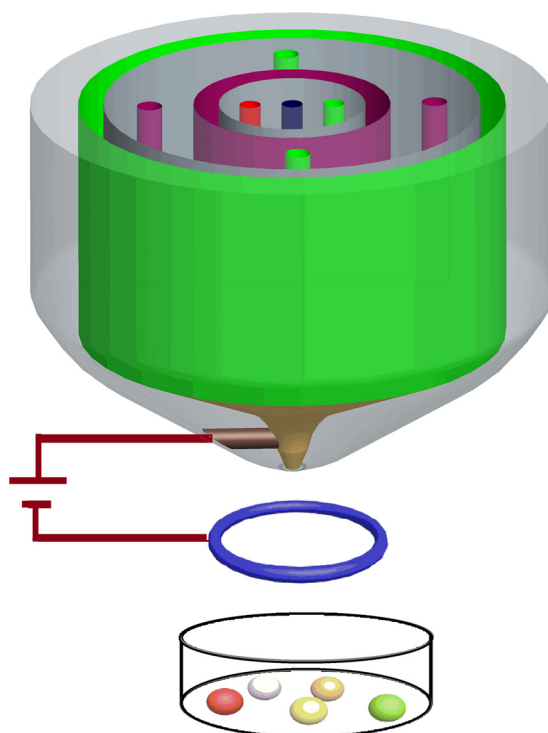
FIG. 1. Sketch of the electrospray setup. Voltage is applied between the nozzle of the 3D device and a grounded ring. A water bath containing 3.0 wt. % calcium chloride solution is used to collect the generated alginate droplets which are simultaneously converted to calcium alginate hydrogel particles.

base material of each deposited layer is then cured by UV light and the supporting material is subsequently removed. With this approach, device-building is done layer-by-layer, resulting in a single-piece device with arbitrarily defined structures in a truly 3D operating space. Channels with numerous shape, size, and height can be conveniently prepared in three-dimensional space. To emphasize this, we design representative millifluidic channel elements with various geometries, ranging from a ring, a hexagon, a star, a tapered funnel to an arbitrarily tortuous channel, with heights as large as centimeters (Fig. 2(a)). These elements can be extended to more complex structures (Fig. 2(b)) easily with no significant increase in fabrication complexity, cost, and time. In contrast, these features are nearly impossible to directly achieve by conventional single-step fabrication techniques. With 3D printing, these configurations can be more conveniently realized by directly designing the structures and transferring to real prototypes, making possible the fabrication of devices as complicated as those with interconnected ring, conical, and round channels as shown in Fig. 2(c). The structures prepared demonstrated the ability to fabricate channels with more sophisticated structures than those prepared using conventional techniques; this will enable researchers to print new channels for applications that require the sophistication not previously achieved.

Besides the high customizability of the channel geometry, the printing quality, such as the resolution and surface roughness, directly affects the reproducibility and size uniformity of the printed particles. To evaluate the printing resolution, a number of channels with different widths and depths, ranging from $80 \mu m$ to $800 \mu m$ have been designed. Channels with sizes larger than $200 \mu m$ can be fabricated for current designs. However, smaller channels cannot be made conveniently due to the large granule size of the precursor powder and the difficulty in completely removing the supporting materials. The printing resolution in x- and y-directions is mainly determined by the hole size of the jetting heads as well as the viscosity and polymerization time of the photopolymer precursor. In our experiments, the printing resolution is around $127 \mu m$ in x- and y-directions. The resolution in z-direction is governed by the step resolution
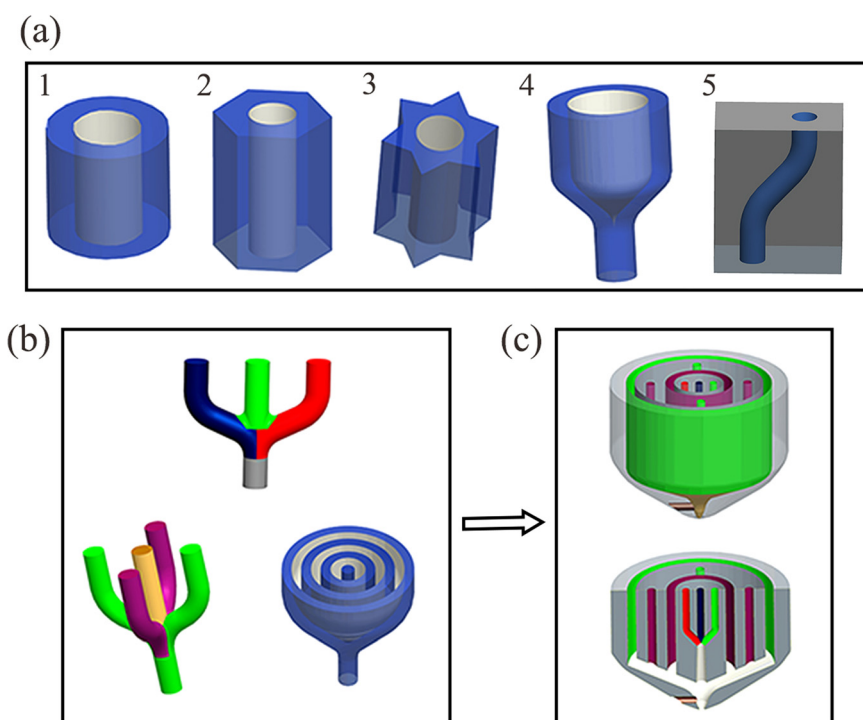
FIG. 2. (a) Representative millifluidic channel elements with heights as large as centimeters and of various geometries: 1, ring; 2, hexagon; 3, star; 4, tapered funnel; 5, arbitrarily tortuous channel; (b) representative extended channel networks. Upper: parallel round channels, bottom left: co-axial round channels and bottom right: concentric ring channels connected to a round channel. (c) Whole configuration and cross-sectional view of a 3D structure with interconnected ring, conical, and round channels at defined locations.

associated with the upward movements of the stage and is around 50 μm. With these resolutions, the minimum feature sizes of our devices are about 1.0 mm. After printing, the solidified structures are still embedded within the remaining supporting material, which can be removed by repeated magnetic stirring and sonication in sodium hydroxide solution. For the channel networks with size around millimeters, the supporting materials can be removed within 1 h. The step for removing the supporting materials becomes more difficult and more time-consuming for devices with smaller, longer, and more tortuous features. This may be a result of the partial polymerization of the supporting material, high flow resistance, and small contact area. Another important feature of printing that affects the final quality of the printed devices is the surface roughness, which is likely related to material properties, such as viscosity and polymerization time, and the step resolution of horizontal movements of the jetting heads. In our devices, the typical roughness is around 10 μm, as measured by a surface profiler. The over-curing of the first layer deposited on the printer tray, or the so-called "back-side effect,"[30] often causes a larger surface roughness in the surface of the printed objects, which touches the printer tray. The problem can potentially be alleviated through reduction of the depth of focus of the exposure light, and optimization of exposure time, wavelength, and printing power.

B. Particle formation through incorporation of electrospray to the 3D-printed nozzles

To prepare multi-compartment particles using droplet-based strategies, there are three main steps, including the generation of a multi-phasic stream, the formation of mono-disperse droplets, and subsequent solidification. 3D millifluidics provides a simple way to generate a multiphasic stream. However, if we simply spray this multiphasic stream in air, droplets will be formed only when the gravitational force and the inertial force exceed the surface tension, which results in a very narrow size range. To better control the droplet size, we apply an electric field to generate the droplets; this provides an additional operating parameter for droplet

formation. The liquid jet will be charged electrically, facilitating its breakup. The droplet formation is then governed by the interplay of electric force, gravity, and surface tension. Here, we show that we can control the droplet size in a wider size range (from 1.4 mm to 4.78 mm) by tuning the electric field strength and total flow rate using the same 3D printed device. For a given flow rate, we can significantly reduce the size of the droplets through increasing the electric field strength (Fig. 3). Besides, at fixed electric field strength, we can reduce the droplet size by decreasing the flow rate (Fig. 3). For droplet generation using electrospray, the droplet size is also significantly influenced by the size of nozzle.[25,30] Smaller nozzle typically results in smaller particles. Due to the limited resolution of our current 3D printer, the minimum feature sizes of our nozzles are about 1.0 mm. However, the size of fabricated particles can be reduced to microscale with a higher-resolution 3D printer. The generation rate of particles for a single nozzle can currently reach over 100 particles per minute, and CV is 4.7%. The generation rate can be easily increased by numbering up the nozzles. This approach does not require any complicated shearing flow or selective surface modification, which are particularly difficult to achieve in devices with complicated geometries. Due to the low fluid velocity, the Reynolds number (Re) is below 1 for millimeter-sized channels. Therefore, turbulent mixing of neighboring solution streams can be avoided.

C. Multi-compartment particles with complex architectures

With our 3D printed electro-millifluidic devices, the patterns of the multiple fluid phases at the nozzle can be customized, enabling breakup of the resultant jet into droplets with corresponding architectures. Upon solidification, the droplets are converted to compartmentalized particles. For example, a round channel can be used to deliver the core fluid, while a ring channel surrounding the round channel can be used for delivering the shell fluid; the resultant drops are then excellent templates for forming core-shell particles (Fig. 4(a)). Numbering up the concentric ring channels can increase the number of shells. The channels for injecting different fluid phases can also be arranged in a parallel fashion for synthesizing particles with compartments arranged in a sandwich-like pattern, or in a radial fashion for particles with compartments arranged in a petal-like pattern (Figs. 4(b) and 4(c)). Each compartment is separated from the neighboring ones by very clear interfaces despite the miscibility of the base alginate solutions before gelation. This clear separation results from the laminar nature of the flows, large viscosity, and the fast gelation of the droplets. There is no observable leeching of the dye
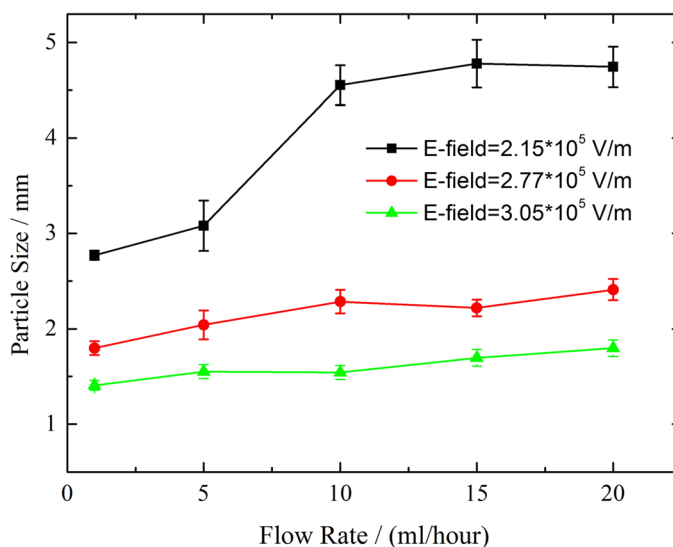

FIG. 3. Effect of electric field strength and flow rate on particle sizes. The size of the particles can be reduced by increasing the electric field or decreasing the flow rate.
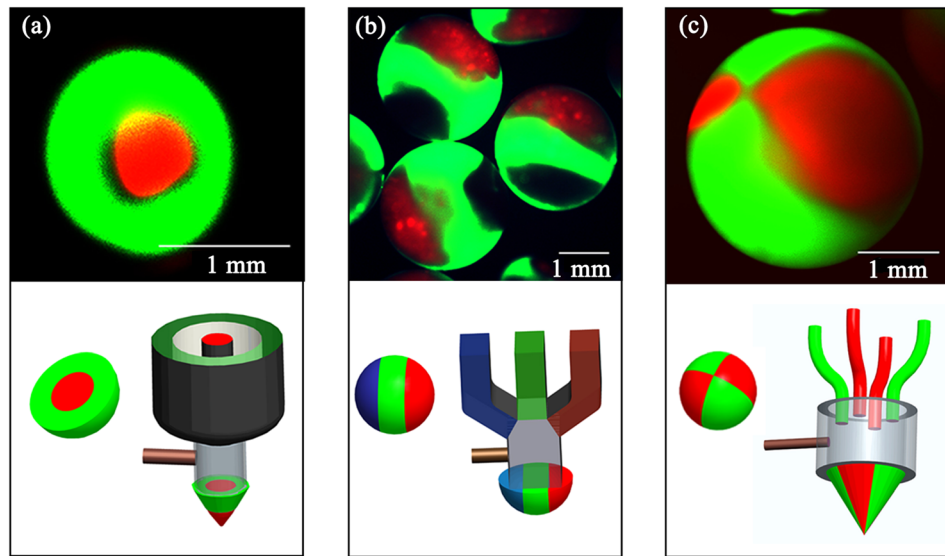
FIG. 4. Fluorescence microscope images of a few particles with (a) two, (b) three, and (c) four compartments arranged in a sandwich-like, core-shell, and petal manner, respectively. Schematics of their corresponding channel geometries are placed below the fluorescent images.

molecules between compartments for more than one week in deionized water at room temperature. The interfaces between compartments remain distinct when the diameter is reduced to around 200 μm, despite the more significant mixing between neighboring compartments, as reported previously in particles prepared without using 3D printing.[30]

The volume ratio between different compartments is proportional to the ratio of the respective flow rates. In addition, the number of compartments can also be easily extended through incorporation of more channel units without increasing the complexity of the device fabrication or particle synthesis. Moreover, with complicated millifluidic structures containing interconnected ring, conical, and round channels, we also obtain distinct hybrid particles containing multiple core-shells with the shells compartmentalized in the corresponding patterns, as shown in Fig. 5. However, with an increasing number of compartments, the volume ratio and the shape of the
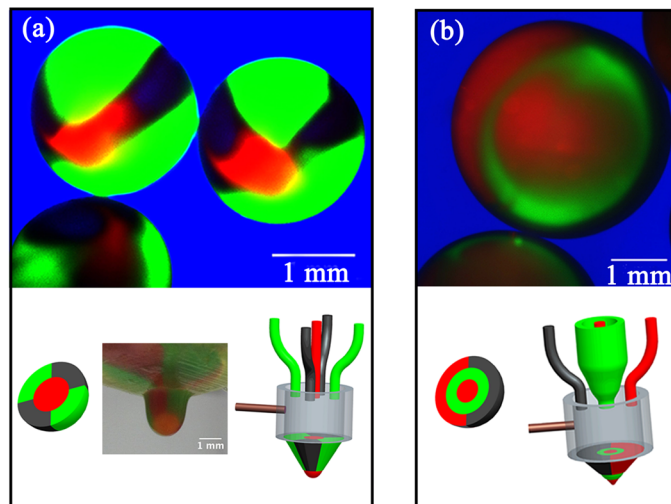

FIG. 5. Fluorescent microscope images of fabricated hybrid particles with structures of (a) a core surrounded by a shell consisting of four petal-like compartments and (b) a core surrounded by a homogeneous shell, which in turn is surrounded by an additional shell consisting of four petal-like compartments.

compartments can become distorted. One possible cause is the fluctuations in the flow rates due to the syringe pump.[42] This problem can potentially be avoided by prolonging the channel length to increase the fluidic resistance and dampen the fluctuations due to the syringe pump.

D. Applications using multi-compartment particles

The different compartments of the particles can be used to load different substances, such as nutrients, drugs, and magnetic materials, providing different functionalities. The quantities and ratio of substances in different compartments depend on the corresponding flow rates. As long as the fluids can be delivered steadily, the quantities and ratio can be made highly consistent. The combination of the different functional components in customized compartments creates new opportunity to prepare novel formulations in food industry, drug delivery and bioassays.

Adults typically have 2000 to 4000 taste buds with diameters of around 80 μm; the numerous sensory cells of each taste bud detects one to several of the five basic tastes, including salty, sour, bitter, sweet, and umami, with varying levels of sensitivity.[43] Up to 100 000 different flavors can be differentiated by each taste bud. Different tastes of food may not be distinctly spatially-differentiated when the ingredients are homogeneously mixed. However, if each ingredient is confined to specific compartments of the particles touching different taste buds of the tongue, different flavors can be sensed in different parts of the tongue. The tasting experience can potentially be quite different from food with homogeneously mixed ingredients. Particles with specifically engineered compartments precisely arranged in space are needed to test this. To demonstrate the degree of control afforded by our approach, we fabricate particles with multiple flavors by encapsulating different fruit juices, including apple, grape, orange, mango, and carrot mixed juices [Minute Maid, Hong Kong], in different compartments of the particles, as shown in Figs. 6(a) and 6(b). If adopted, our approach will allow formulation of food components with more sophisticated tastes through unique combinations of multiple ingredients.

In drug delivery, two or more drugs with different properties often need to be administered simultaneously for enhanced therapeutic effects. For instance, in the treatment of tuberculosis, co-encapsulation of isoniazid and rifampicin leads to enhanced encapsulation efficiency and extended drug release.[44] The production of our sophisticated particles may allow for applications, including drug co-delivery and cell-related studies if the particle size is reduced to the microscale with a higher-resolution 3D printer. Drugs with structures and molecular weight comparable to the model fluorescent molecules should also remain isolated from each other in different compartments, similar to the confinement of fluorescent molecules shown in Figs. 4, 5 and 6(b). Using our multi-compartment particles, multiple drugs can be separately encapsulated to different compartments and delivered to the target tissues or organs before their simultaneous release. As a demonstration of the ability to co-encapsulate, we use vitamin C (Vc) and APL as model drugs and study the release kinetics. We encapsulate Vc in the cores and APL in the two symmetrical petals forming the outer shell, respectively, of the multi-compartment particles prepared using our approach. The two drugs are rapidly released from the particles with a large initial burst rate due to large pore sizes of the alginate hydrogel, without interference with each other (Fig. 6(c)). There is no degradation of the drugs at least for over 4 h (Fig. S3 in the supplementary material).[40] Particles made of similar material can be stored for around 6 months in deionized water at room temperature.[45] As our approach only involves physical mixing of the different fluidic streams, without introducing any new materials chemistry, the properties of the matrix materials that form the particle, including its degradability, leeching, and potency of active ingredients, should remain the same as those materials investigated previously. The outer shell has been demonstrated to modulate the release kinetics of drugs encapsulated in inner cores as a buffer layer.[17] Further modulation of the release dynamics can be realized by introducing hydrogel precursors of different concentrations to different compartments, thereby tuning the permeability of the different compartments and consequently the release profile;[45–47] or by injecting different binding agents, such as ligands, in the different compartments for binding drugs with different strengths, thereby modifying the release profile.[48] Both of these strategies
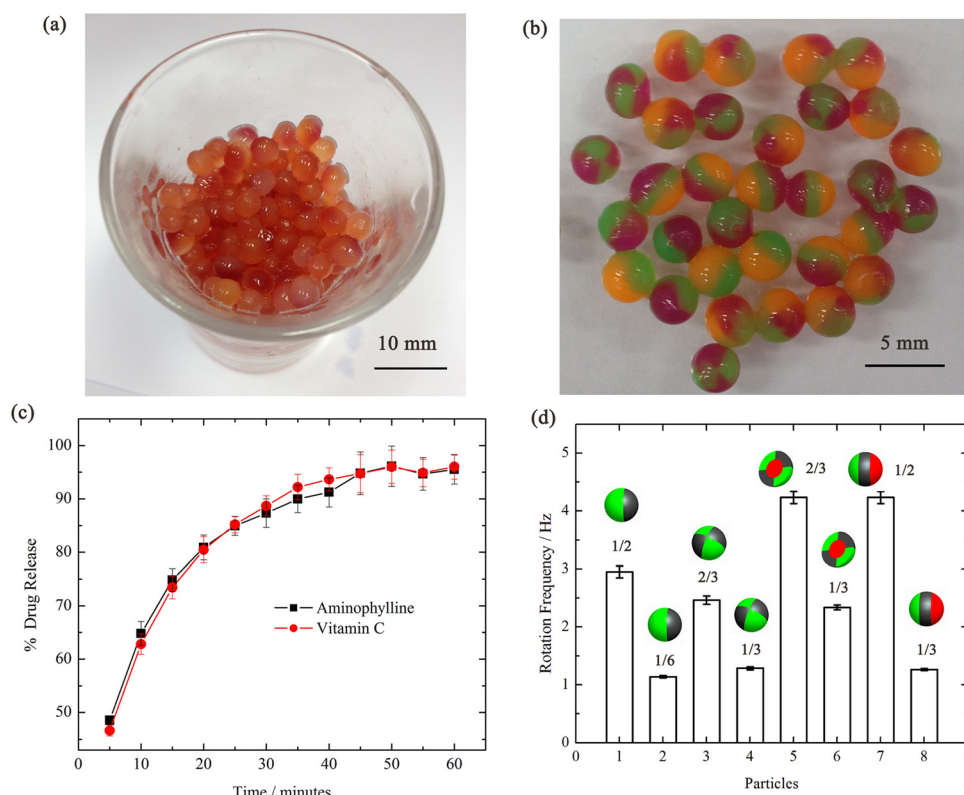
FIG. 6. Photographs of (a) particles encapsulating different juices in different compartments, and (b) particles encapsulating different juices mixed with different dyes for visualization of the compartmental structures. (c) Release profile of vitamin C and aminophylline co-encapsulated in different compartments of particles, (d) rotational speed of particles with iron (III) oxide nanoparticles loaded into the grey compartments as denoted in the illustration above the bars in the histogram. The red and green compartments represent different compartments consisting of crosslinked alginate and other components to be encapsulated. The fraction above the bars refers to the volume fraction of the magnetized volume to total volume. All particles used are placed in close proximity to a magnetic stirrer rotating at 800 rpm.

are enabled by the exquisite control over the device architecture and the resultant particle shapes with the 3D printing-based electro-millifluidic devices. By extending the range of particle structures, for instance, by varying the number of shells and compartments as discussed above, our approach may allow the modulation of the co-release of multiple drugs for therapeutic applications.

Apart from encapsulation for subsequent release, functional components are often encapsulated to enhance the performance of the multi-compartment particles. For instance, magnetized nanoparticles are widely used for tracking in bioassays.[49,50] The ability of our approach to customize the architectures of the particles allows confinement of these magnetized nanoparticles into sophisticatedly arranged compartments. By varying the arrangement of the magnetized particles, the motion of the particles can be precisely adjusted. To demonstrate this, we prepare multi-compartment alginate particles with iron (III) oxide nanoparticles arranged in different compartments (Fig. 6(d)). Under a constant rotating magnetic field provided by a magnetic stirrer, the particles rotate at a constant speed, independent of the initial position of the particles on the stirrer plate (Fig. S4 in the supplementary material).[40] With different arrangements and structures of the magnetized compartments, the rotational speeds differ. For instance, the hybrid core-shell particles with nanoparticles loaded to the symmetric petals at the outer shell rotate faster than the petal particles with nanoparticles loaded to the symmetric petals without a core, and the sandwich-like particles with the middle slice magnetized rotate faster than Janus particle with only one face magnetized, as shown in Fig. 6(d). Besides, the volume fraction of the magnetized compartments over total volume can also change the rotational speed. For the same

magnetized structure of the particles mentioned above, increasing the volume fraction results in a higher rotational speed. Since the arrangement and structures of magnetized compartments change the position of the equivalent magnetized center, while the volume fraction changes the mass fraction of the magnetic particles, the resultant torque that determines the rotational speed changes accordingly. Our versatile 3D printed electro-millifluidic approach enables excellent control over the attributes of the multi-compartment particles. The simple and scalable approach allows preparation of particles with tunable magnetized configuration and size for use as components of passive valves, and as mini-actuators with asymmetrically arranged magnetic compartments.

IV. CONCLUSION

In this paper, we introduce 3D printing to fabricate millifluidic devices with electrodes embedded for fabricating droplets with complex structures and tunable sizes. Tedious procedures in conventional microfabrication methods, such as alignment, bonding, and assembly, are not required. Using the droplets with sophisticated architectures as templates, we fabricate compartmentalized particles with designer structures. Our 3D printed electro-millifluidic approach represents a simple and versatile method to extend the range of structures of functional particles. These particles can be used to separately encapsulate various substances, including nutrients, drugs, and magnetic particles, for co-delivery and actuation in applications ranging from food to drug delivery and to bioassays.

ACKNOWLEDGMENTS

[1] J. Čejková and F. Štěpánek, Curr. Pharm. Des. **19**, 6298–6314 (2013).
[2] J. Z. Du and R. K. O. Reilly, Chem. Soc. Rev. **40**, 2402–2416 (2011).
[3] K. Maeda, H. Onoe, M. Takinoue, and S. Takeuchi, Adv. Mater. **24**, 1340–1346 (2012).
[4] Q. P. Pham, U. Sharma, and A. G. Mikos, Biomacromolecules **7**, 2796–2805 (2006).
[5] N. Sakata, S. Sumi, G. Yoshimatsu, M. Goto, S. Egawa, and M. Unno, World J. Gastrointest. Pathophysiol. **3**, 19–26 (2012).
[6] S. Rahmani and J. Lahann, MRS Bull. **39**, 251–257 (2014).
[7] D. Dendukuri and P. S. Doyle, Adv. Mater. **21**, 4071–4086 (2009).
[8] J. H. Kim, T. Yoon Jeon, T. M. Choi, T. S. Shim, S. H. Kim, and S. M. Yang, Langmuir **30**, 1473–1488 (2014).
[9] D. C. Appleyard, S. C. Chapin, R. L. Srinivas, and P. S. Doyle, Nat. Protoc. **6**, 1761–1774 (2011).
[10] W. Engl, R. Backov, and P. Panizza, Curr. Opin. Colloid Interface Sci. **13**, 206–216 (2008).
[11] L. Baraban, F. Bertholle, M. L. M. Salverda, N. Bremond, P. Panizza, J. Baudry, J. G. M. Visserb, and J. Bibettea, Lab Chip **11**, 4057–4062 (2011).
[12] W. J. Duncanson, A. Abbaspourrad, H. C. Shum, S. H. Kim, L. L. A. Adams, and D. A. Weitz, Langmuir **28**, 6742–6745 (2012).
[13] L. Zhang, S. C. Hao, B. Liu, H. C. Shum, J. Li, and H. S. Chen, ACS Appl. Mater. Interfaces **5**, 11489–11493 (2013).
[14] W. Wang, M. J. Zhang, and L. Y. Chu, Acc. Chem. Res. **47**, 373–384 (2014).
[15] C. H. Chen, A. R. Abate, D. Lee, E. M. Terentjev, and D. A. Weitz, Adv. Mater. **21**, 3201–3204 (2009).
[16] H. C. Shum, Y. J. Zhao, S. H. Kim, and D. A. Weitz, Angew. Chem. Int. Ed. **50**, 1648–1651 (2011).
[17] J. Wu, T. T. Kong, K. W. K. Yeung, H. C. Shum, K. M. C. Cheung, L. Q. Wang, and M. K. T. To, Acta Biomater. **9**, 7410–7419 (2013).
[18] Y. D. Hu, J. Y. Wang, H. Wang, Q. Wang, J. T. Zhu, and Y. J. Yang, Langmuir **28**, 17186–17192 (2012).
[19] T. T. Kong, Z. Liu, Y. Song, L. Q. Wang, and H. C. Shum, Soft Matter **9**, 9780–9784 (2013).
[20] P. Agarwal, S. Zhao, P. Bielecki, W. Rao, J. K. Choi, Y. Zhao, J. Yu, W. Zhange, and X. M. He, Lab Chip **13**, 4525–4533 (2013).
[21] Z. H. Nie, W. Li, M. Seo, S. Q. Xu, and E. Kumacheva, J. Am. Chem. Soc. **128**, 9408–9412 (2006).
[22] Q. B. Xu, M. Hashimoto, T. T. Dang, T. Hoare, D. S. Kohane, G. M. Whitesides, R. Langer, and D. G. Anderson, Small **5**(13), 1575–1581 (2009).
[23] T. Franke, A. R. Abate, D. A. Weitz, and A. Wixforth, Lab Chip **9**, 2625–2627 (2009).
[24] M. Hashimoto, S. S. Shevkoplyas, B. Zasońska, T. Szymborski, P. Garstecki, and G. M. Whitesides, Small **4**, 1795–805 (2008).

[25]J. Lahann, Small **7**, 1149–1156 (2011).
[26]L. Zhang, J. Huang, T. Si, and R. X. Xu, Expert Rev. Med. Devices **9**(6), 595–612 (2012).
[27]Z. Ahmad, H. B. Zhang, U. Farook, M. Edirisinghe, E. Stride, and P. Colombo, J. R. Soc. Interface **5**, 1255–1261 (2008).
[28]H. F. Yang, X. Qiao, W. Hong, and L. Dong, J. Microelectromech. Syst. **22**, 509–518 (2013).
[29]R. F. Shepherd, J. C. Conrad, S. K. Rhodes, D. R. Link, M. Marquez, D. A. Weitz, and J. A. Lewis, Langmuir **22**, 8618–8622 (2006).
[30]Z. Liu and H. C. Shum, Biomicrofluidics **7**, 044117 (2013).
[31]K. H. Roh, D. C. Martin, and J. Lahann, Nat. Mater. **4**, 759–763 (2005).
[32]K. H. Roh, D. C. Martin, and J. Lahann, J. Am. Chem. Soc. **128**, 6796–6797 (2006).
[33]G. Comina, A. Suska, and D. Filippini, Lab Chip **14**, 424–430 (2014).
[34]P. J. Kitson, M. H. Rosnes, V. Sans, V. Dragone, and L. Cronin, Lab Chip **12**, 3267–3271 (2012).
[35]A. I. Shallan, P. Smejkal, M. Corban, R. M. Guijt, and M. C. Breadmore, Anal. Chem. **86**, 3124–3130 (2014).
[36]J. L. Erkal, A. Selimovic, B. C. Gross, S. Y. Lockwood, E. L. Walton, S. McNamara, R. S. Martinb, and D. M. Spence, Lab Chip **14**, 2023–2032 (2014).
[37]A. K. Au, W. Lee, and A. Folch, Lab Chip **14**, 1294–1301 (2014).
[38]S. Z. Guo, F. Gosselin, N. Guerin, A. M. Lanouette, M. C. Heuzey, and D. Therriault, Small **9**, 4118–4122 (2013).
[39]K. G. Lee, K. J. Park, S. Seok, S. Shin, D. H. Kim, J. Y. Park, Y. S. Heo, S. J. Lee, and T. J. Lee, RSC Adv. **4**, 32876–32880 (2014).
[40]See supplementary material at http://dx.doi.org/10.1063/1.4902929 for the supplementary figures and videos.
[41]http://www.stratasys.com/3d-printers/technologies/polyjet-technology.
[42]Z. D. Li, S. Y. Mak, A. Sauret, and H. C. Shum, Lab Chip **14**, 744–749 (2014).
[43]http://www.ncbi.nlm.nih.gov/pubmedhealth/PMH0033701/.
[44]A. Gürsoy, E. Kut, and S. Özkırıml, Int. J. Pharm. **271**, 115–123 (2004).
[45]N. Abubakr, A. Jayemanne, N. Audrey, S. X. Lin, and X. D. Chen, Asia Pac. J. Chem. Eng. **5**, 804–810 (2010).
[46]N. Bhattarai, J. Gunn, and M. Q. Zhang, Adv. Drug Delivery Rev. **62**, 83–99 (2010).
[47]T. R. Hoare and D. S. Kohane, Polymer **49**(8), 1993–2007 (2008).
[48]L. Yang and P. Alexandridis, Curr. Opin. Colloid Interface Sci. **5**, 132–143 (2000).
[49]G. Beaune, B. Dubertret, O. Clment, C. Vayssettes, V. Cabuil, and C. Menager, Angew. Chem. Int. Ed. **46**, 5421–5424 (2007).
[50]F. Aldeek, X. Ji, and H. Mattoussi, Phys. Chem. C **117**, 15429–15437 (2013).